JOURNAL OF PROPULSION AND POWER
Vol. 26, No. 1, January–February 2010

Supersonic Boundary-Layer Combustion: Effects of Upstream Entropy and Shear-Layer Thickness

Rainer M. Kirchhartz,* David J. Mee,† Raymond J. Stalker,‡ Peter A. Jacobs,§ and Michael K. Smart¶
University of Queensland, Brisbane, Queensland 4072, Australia

DOI: 10.2514/1.44485

There is much interest in the way in which fuel is injected into scramjet combustors and the way this influences ignition and combustion. Experiments were conducted in the T4 Stalker Tube to assess the combustion of hydrogen when it is injected directly into the boundary layer of a circular constant-area supersonic combustion chamber ($M > 4$). The wall-layer conditions at the fuel-injection station were varied to study the effects on the ignition and combustion of the injected hydrogen. This was achieved by varying the leading-edge bluntness and the length of the constant-area inlet upstream of the annular fuel-injection slot that delivers fuel as a layer underneath the existing boundary layer. Flow properties at the injection location calculated using computational fluid dynamics are presented as well as experimental data and analytical predictions of the pressure distributions along the combustion chamber wall. It is shown that a thicker boundary layer promotes combustion and that leading-edge bluntness, which leads to more hot gas near the walls, is more effective for ignition.

Nomenclature

c_p	=	pressure coefficient, $(p - p_\infty)/q_\infty$
H	=	enthalpy
h	=	altitude
L	=	length scale, length of inlet
M	=	Mach number
p	=	static pressure
q	=	dynamic pressure
R	=	radius
R_n	=	leading-edge radius
T	=	temperature
U_{typ}	=	typical uncertainty
u	=	velocity
u_s	=	incident shock speed
x	=	axial position
γ	=	ratio of specific heats
η_c	=	combustion efficiency
$\eta_{c,\text{tot}}$	=	total combustion efficiency
η_m	=	mixing efficiency
ρ	=	density
ϕ	=	fuel equivalence ratio
ϕ_{eff}	=	effective fuel equivalence ratio

Subscripts

f	=	flight condition
fill	=	initial tube fill property
j	=	fuel jet property
0	=	stagnated or total property
2, 3, 4	=	station designation for cycle analysis
∞	=	freestream property

Received 20 March 2009; revision received 17 August 2009; accepted for publication 17 August 2009.

*Ph.D. Student, School of Mechanical and Mining Engineering. Student Member AIAA.
†Professor, School of Mechanical and Mining Engineering. Associate Fellow AIAA.
‡Emeritus Professor, School of Mechanical and Mining Engineering. Fellow AIAA.
§Senior Lecturer, School of Mechanical and Mining Engineering.
¶Professor, School of Mechanical and Mining Engineering. Senior Member AIAA.

I. Introduction

THE autoignition of fuel in a scramjet combustor is strongly influenced by the temperature and pressure of the gas into which the fuel is injected. How the fuel subsequently mixes and burns is also affected by the way in which the fuel is introduced into the flow. Injection from struts positioned in the core flow can result in good mixing but incurs large wave-drag losses [1,2] and problems with high heating rates to the injector [3–5]. Some of these problems can be reduced by injecting fuel from holes normal or inclined to the surface [5,6] or from structures attached to the surface [5]. Injection from inclined wall fuel jets into the mainstream flow in the combustor can provide good mixing, but can also result in large momentum losses as the flight Mach number increases and the fuel momentum becomes a significant fraction of the engine thrust [3,7]. A less disruptive injection method is tangential wall slot injection of the fuel [3], but this can be difficult to ignite [8] and may result in low combustion efficiencies [5,9]. However, this method can also be an efficient means to reduce surface heat loads [10] and internal surface drag [11].

Some of the factors limiting combustion with wall injection of fuel are ignition of the fuel and the mixing of the fuel with the air passing through the combustor. Although the mean temperature of the flow within a combustor may not be high enough for ignition of the fuel, combustion can be initiated in regions of locally high temperature and pressure [3,12]. Boundary layers formed on the walls of an intake and entropy layers caused by blunted leading edges can produce such regions of high temperature [13]. In this paper, we report results of experiments designed to investigate the influence of the oncoming wall layer flow upstream of the location of tangential injection of hydrogen on both the ignition of the fuel and the amount of fuel that mixes and burns.

Previous work with supersonic tangential slot injection of hydrogen into a supersonic airstream has shown that the boundary-layer thickness at the point of injection plays an important role in the ignition of the mixture. In [8], a constant-area circular duct was used. The boundary layer was laminar at the point of injection and its thickness was of the order of a quarter of the slot height. It was observed that the fuel did not ignite quickly. In contrast, when the fuel was injected into a turbulent boundary layer with a thickness of the order of the slot height, the fuel ignited and burned more quickly [14]. Numerical calculations supported the deduction that the thicker,

turbulent boundary layer resulted in more hot air that was available to mix with fuel, promoting ignition and combustion [15]. A theoretical analysis given in [16] comes to the same conclusion.

A thick entropy layer can also influence the surface flow. Such an entropy layer can result in a thick layer of hot gas near or inside the boundary layer [13] and it can be generated by a blunt leading-edge bow shock. This may influence combustion of hydrogen in a similar manner to a thick boundary layer. This configuration is particularly interesting as hypersonic flight vehicles will most likely incorporate somewhat blunted leading edges to reduce heating loads [13].

The aims of the present study are to investigate experimentally the influence on ignition and combustion of 1) the thickness of the turbulent or laminar boundary layer at the point of injection, and 2) bluntness of the leading edge upstream of the point of injection, when fuel is injected tangentially along the combustor wall. To achieve the first aim, the experimental apparatus is that of [8], modified to allow alteration of the boundary-layer thickness at injection. This ensures that no other effects influence the comparison between the thick and thin boundary-layer data. To achieve the second aim, the same configuration was also fitted with blunted leading edges to investigate the effect of entropy layers on the boundary-layer combustion. The experiments reported here are relevant for scramjet combustors at flight Mach numbers in excess of eight, where the Mach number at entry to the burner is in excess of four.

The inlet and combustor walls were not heated for the presented experiments. Previous investigations have not found a strong influence of the wall temperature on the ignition of wall portholes injected hydrogen [17]. This is supported by the relative insensitivity of the maximum temperature in the boundary layer to the temperature of the wall in hypersonic flows where the wall temperature is lower than the mainstream temperature (this can be shown, for example, using Eqs. 34 and 72 of [18]). However, it is possible that the present configuration is more sensitive to wall temperatures because fuel injection and combustion are close to the wall. Hot walls alter the boundary layer upstream of injection and the wall fuel jet and may influence ignition and combustion characteristics. This effect is not addressed in the current project.

II. Model Configuration

The experiments were conducted in the T4 Stalker Tube [19], using a Mach 4 contoured nozzle [20]. The shock-tunnel model consisted of a circular combustion chamber with an internal diameter of 33.2 mm and a length of 500 mm. Upstream of the combustion chamber is a constant-area inlet of 60.5 or 244.5 mm length and 28.8 mm internal diameter. The rearward-facing step formed by the diameter change accommodates an annular slot injector for the gaseous hydrogen fuel as shown in Fig. 1. There were two versions of the short and long inlets, one set with sharp leading edges and one with 0.5 mm radii. Figure 2 shows an overall view of the shock-tunnel model. The nozzle exit core flow provided the inlet entry flow, creating a quasi-direct connect-testing arrangement without any scramjet inlet compression. Because the nozzle expansion varies with the total enthalpy of the gas and it was not operated at the original design condition, the nozzle exit Mach number was close to 4.5 for the present conditions.

The fuel-injection slot was of annular cross section with a 17 deg half-cone angle at the sharp trailing edge. Twenty static pressure

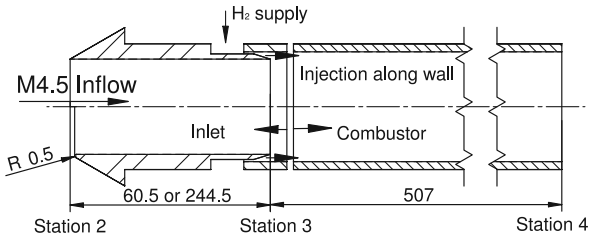

Fig. 1 Schematic of the inlet-combustor arrangement, shown with sharp (top) and blunt (bottom) leading edge, dimensions in millimeters.

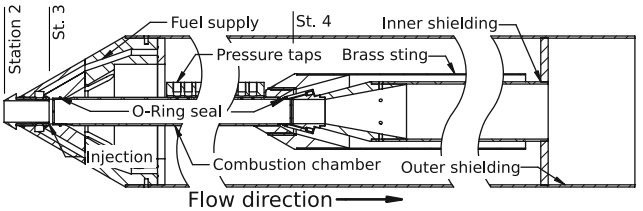

Fig. 2 Layout of the stress-wave force balance with combustion chamber for pressure measurements, shown with sharp leading edge, short inlet configuration.

tappings at 15 mm spacing in the wall of the combustion chamber were used to measure pressures in the combustor; the first was located approximately 170 mm downstream of the injection plane.

The model was designed to allow the measurement of skin-friction drag on the combustion chamber walls while all other forces are decoupled. This necessitates the relatively high level of complexity of the model in comparison to that which would otherwise be needed if only pressure measurements were taken. These drag measurements are reported elsewhere [21].

III. Computational Approach

A. Computational Fluid Dynamics Simulations

In the process of designing the model for the wind-tunnel tests, some numerical simulations were performed using the multiblock compressible Navier–Stokes solver MB_CNS [22]. Only the constant-area duct upstream of the annular injection slot was modeled. The results of these simulations were used to determine the effects of different inlet configurations on the flow properties at the injection plane. As an indication of the solved flowfields, some comparisons of pressure contours for sharp and blunt leading edges are given in Figs. 3 and 4. The calculations for the short inlet configurations were performed assuming a fully laminar boundary layer, whereas the calculations for the long inlet configurations included forced boundary-layer transition occurring 120 mm downstream of the leading edge. This corresponds to a transition Reynolds number of approximately 2×10^6 and is based on previous boundary-layer transition experiments performed in the T4 shock tunnel [23,24]. Turbulence effects were modeled using the Baldwin–Lomax [25]

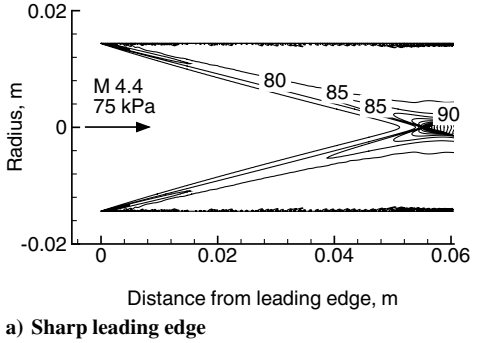

a) Sharp leading edge

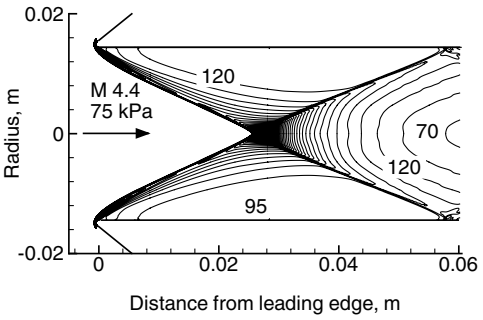

b) 0.5 mm radius leading edge

Fig. 3 Pressure contours for the short inlet configuration flowfield with sharp and blunt leading edge. Contour values shown are in kilopascals.

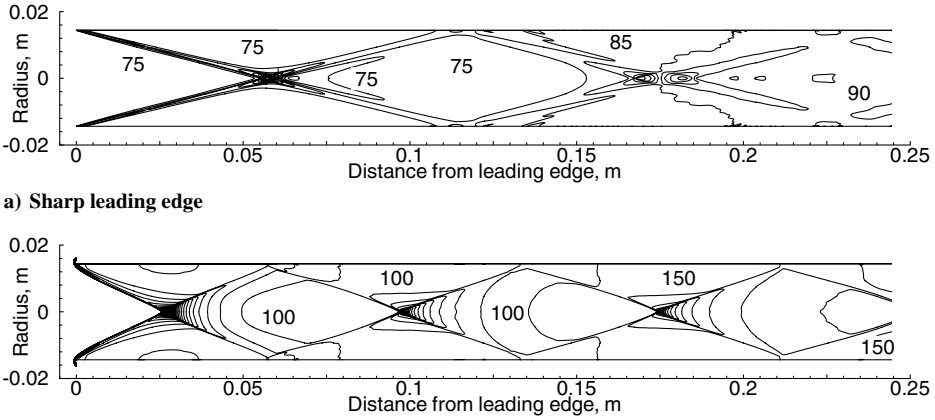

a) Sharp leading edge

b) 0.5 mm radius leading edge

Fig. 4 Pressure contours for the long inlet configuration flowfield with sharp and blunt leading edge. Contour values shown are in kilopascals.

turbulence model. A total of 80,400 cells were used for the simulation of the short blunt inlet configuration and 163,600 cells for the corresponding long inlet configuration. A grid resolution study for these simulations demonstrated that this grid was adequate to resolve the shock layers and that the flow profiles across the duct are mesh independent. According to the Korkegi boundary-layer separation criterion [26], the pressure rise over the shock impingement points on the wall is not sufficient to cause separation of the boundary layer. The pressure at the injection plane is almost doubled by the use of a blunted leading edge compared with the sharp leading-edge case.

Figure 5 shows the radial profile of density and temperature from the centerline ($R = 0$ mm) to the inlet wall ($R = 14.4$ mm) for different inlet configurations, and Fig. 6 illustrates the effect of flow total enthalpy on those profiles.

Examination of the profiles in Fig. 5a indicates that the blunted leading edge on the short inlet results in the highest peak temperature near the wall. This is most likely caused by the coincidence of the entropy layer and the reflected leading-edge shock as shown in Fig. 3b. The long inlet with a sharp leading edge provides a higher near-wall temperature than the short sharp inlet, but more importantly, also generates a significantly thicker hot boundary layer. Generally, blunt leading edges and long inlets result in broader wall layers with high temperatures. Comparison of the temperature profiles plotted in Fig. 6a shows that when the leading edge is blunted, the temperature near the wall for a lower enthalpy flow ($H_0 = 3.9$ MJ/kg, $R_n = 0.5$ mm) can be higher and the region of hot gas thicker than for a higher enthalpy flow with a sharp leading edge ($H_0 =$ 3.9 MJ/kg, $R_n = 0.0$ mm). The thickness of this wall layer and the ratio of the temperature in the mainstream to the peak temperature in the wall layer stay approximately constant when the mainstream temperature is changed. The elevated temperature along the wall could cause an inherent reduction of the fluid's density, which would be detrimental to ignition delay times [27] and could offset some of the reduction in ignition delay time that is caused by the increased

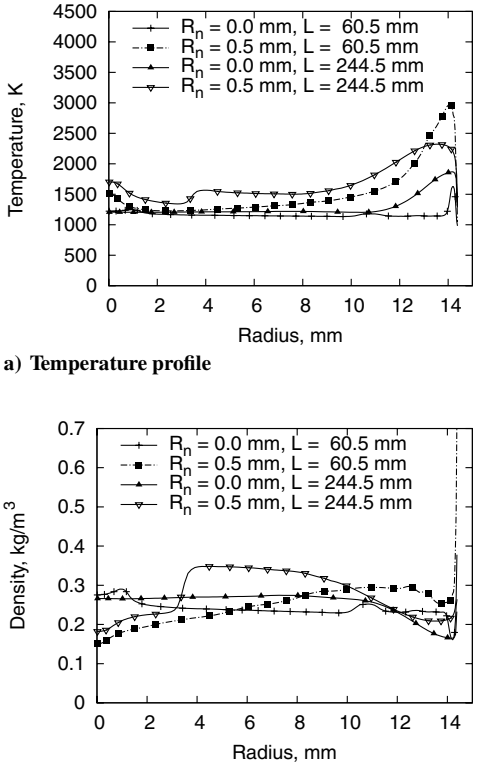

a) Temperature profile

b) Density profile

Fig. 5 Cross-stream profiles of static temperature and density at the fuel-injection location for some different inlet configurations at $H_0 = 5.9$ MJ/kg.

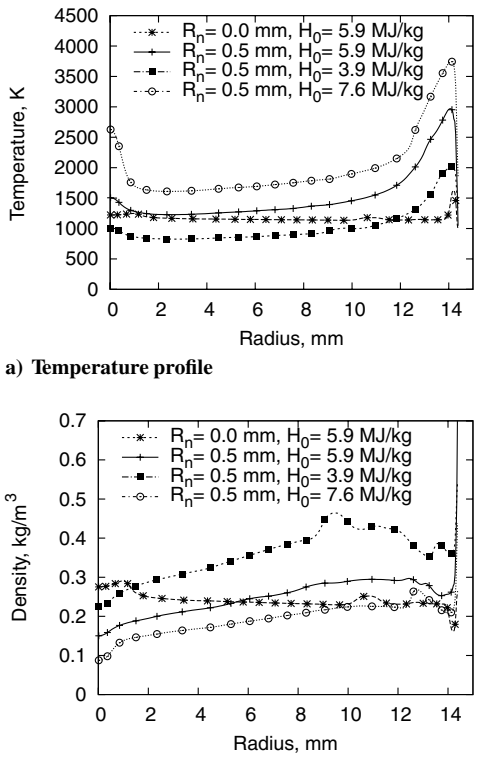

a) Temperature profile

b) Density profile

Fig. 6 Variation of temperature and density at the injection location with bluntness and total enthalpy (short inlet).

temperature. However, as Fig. 5b shows, the wall-layer densities of the blunted leading-edge configurations are higher than those of the colder sharp leading-edge configurations. This is also the case when the mainstream density is significantly reduced by increasing the mainstream total enthalpy (see Fig. 6b). It is therefore expected that the blunted leading edge will enhance ignition and combustion of the wall-injected fuel. The abrupt changes in the flow property profiles (Fig. 5 and 6) are due to the oblique shocks generated by the blunt leading edge.

B. Quasi-One-Dimensional Cycle Analysis

Mixing and combustion processes in a supersonic flow environment with fuel injection (nonpremixed) are very complex and usually highly three-dimensional and nonuniform. A detailed analysis of these phenomena is therefore very costly and complex. A simple, yet very useful, approximate engineering approach is cycle analysis with stream-thrust averaging of the engine and/or combustor flowfield [28,29] For stream-thrust averaged analyses, the mass, momentum, and energy are conserved throughout the flowfield, but the flow properties are averaged and assumed to be constant across the duct at any axial location. The flow is thus assumed to be quasi-one-dimensional, and combustion is usually modeled by heat addition over a specified length of the duct.

A number of previous workers have successfully used this type of analysis to assess performance of scramjet combustors (for example [30–33]). The main use has been the parametric study of scramjet combustor design, but some successful applications involved the postexperiment analysis of combustion tests [31,32,34]. Billig [3,35] and Heiser and Pratt [36] warn that, particularly in dual-mode combustion systems, this approach of outside–in analysis only yields sensible results for low-effective equivalence ratios $\phi_{\text{eff}} = \phi \times \eta_{c,\text{tot}}$. However, no upper bound for this measure of the total amount of fuel that is consumed was given. As a result, the findings of the quasi-one-dimensional analysis that are presented here are to be taken with caution and more as a qualitative than quantitative indication of the amount of fuel that was consumed in the combustor, particularly those that indicate a high-effective equivalence ratio.

The perfect gas version of the quasi-one-dimensional cycle analysis computer program used for this study is described in [37]. In the current version the combustor flow is modeled as a mixture of thermally perfect gases that are in thermodynamic equilibrium. The mixing of fuel and air is specified via a mixing efficiency curve $\eta_m(x)$ and the combustion process is assumed to be mixing limited. This means that once the fuel is allowed to mix with the air, the mixture immediately reaches an equilibrium state of fuel, air, and combustion products. The mixing efficiency η_m is hence the same as the combustion efficiency η_c. The analysis is carried out between stations 2 and 4 with fuel injection at station 3 (see Fig. 1). Flow compression due to boundary-layer growth is modeled by assuming a constant skin-friction coefficient of 0.002 along the wall, which reduces the mainstream momentum and leads to increasing pressures along a constant-area duct.

Because a one-dimensional analysis is unable to model the effects of the oblique shocks that are generated by the blunted leading edges, a way of accounting for their effects has to be incorporated. These shocks are much stronger than those caused by the viscous interaction for the sharp-edged intake (compare Figs. 3 and 4). To account for these effects, perfect gas computational fluid dynamics (CFD) simulations of the inlet geometry were performed for each of the nominal test conditions as given in Table 1. The flow properties were extracted at the fuel-injection station (station 3 in Fig. 1) and the fluid in that plane was allowed to mix in a stream-thrust averaging procedure [29]. The resulting ratios of the freestream and the averaged injection plane flow properties were used to scale the freestream properties of the individual experiments to account for shot-to-shot variations and thus obtain an estimate of the combustor entry conditions. For these cases, the one-dimensional cycle analysis was started at station 3 rather than station 2 (see Fig. 1).

For the present work, this cycle analysis was used to estimate what fraction of the injected hydrogen would have to combust to yield the pressure rise that was measured experimentally. Note that pressure measurements were only available from 170 mm downstream of the injection point. Therefore, in most cases the actual point of ignition and initial pressure rise could not be obtained. Total mixing efficiencies of 0.0 and 1.0 correspond, respectively, to no combustion and complete combustion of the injected hydrogen. Because the analysis does not include nonequilibrium chemistry effects, the combustion reactions are always assumed to be completed. Low reaction rates are not accounted for. Therefore, the fraction of the injected hydrogen that this cycle analysis allows to react releases its entire reaction heat. It is possible that a larger portion of the injected hydrogen is involved in reactions, but that not all reactions are complete and only partially release the available chemical energy. The reported combustion efficiencies are, therefore, to be taken as the equivalent mass fraction of hydrogen that would yield the required chemical heat release to cause the measured pressure rise.

Table 1 Nominal experimental test conditions entering the model and equivalent flight conditions

	Experimental condition						Flight equivalent		
	H_0	p_∞	T_∞	ρ_∞	u_∞	M_∞	$M_{f,\infty}$	h_f	q_f
	MJ/kg	kPa	K	mg/m^3	m/s	——	——	km	kPa
A	3.6	84.0	780	0.370	2420	4.36	8.4	38	17
B	5.3	82.3	1100	0.257	2900	4.47	10	39	25
C	6.4	88.5	1360	0.226	3125	4.38	12	37	40
D	7.9	100.0	1780	0.197	3380	4.22	13	33	85
U_{typ}	8%	13%	9%	11%	3%	2%			

IV. Flow Conditions for the Experiments

A. Freestream

Experiments were performed using test gases of air or nitrogen. The nitrogen cases were used to investigate the effects of fuel-injection without combustion. The nozzle-supply enthalpy was varied from 3.6 to 7.9 MJ/kg with freestream static pressures of 82–100 kPa. These conditions correspond to combustor conditions that might be expected for flight at Mach numbers from around 8 to 13 at altitudes from 30 to 40 km. The nominal test conditions entering the model (station 2) along with their respective equivalent flight conditions are given in Table 1. The nozzle-supply enthalpy was varied within each experimental set for the different inlet configurations to determine a freestream flow condition at which the fuel would ignite in this particular configuration. The dynamic pressure at combustor entry was held approximately constant.

The equivalent flight conditions were obtained by relating the conditions in the combustor to those that might be expected in the combustor of a full-scale flight vehicle. They are provided as a relevant context for hypersonic flight environments. Density-length ρL scaling [38] was used to relate the present inlet radius and pressure to those of a scramjet engine that was used in a recent study on orbital delivery of small payloads [39]. Shock-tunnel scaling experiments have previously shown the applicability of ρL scaling for supersonic duct combustion [40]. The combustor entry radius R_2 was chosen as the scaling length. The scramjet incorporated in [39] has an elliptical combustion chamber with a rectangular to elliptical shape transition inlet. The cross-sectional area of the combustor entry ellipse was used to find the radius of a circle with the same area ($R_{2,f} = 117$ mm). If the ideal gas law is assumed valid and T is to be duplicated in the combustion chamber, $\rho L = \text{const.}$ is equivalent to $pL = \text{const.}$ With $R_2/R_{2,f} = 14.4/117$ it follows that $p_{2,f} = 0.123 p_2$. The freestream flight conditions (Mach number and altitude) that would produce the combustor conditions were found by accounting for inlet kinetic energy efficiency (see Eq. 57 in [41] and Eq. 57 in [28], Sec. 5.3). The ratio of specific heats γ was assumed constant at 1.36 for the compression process [28]. The international standard atmosphere was used to determine the air properties as a function of altitude [42].

The freestream properties were not measured directly in the test section, but were inferred from other measurements. The operating

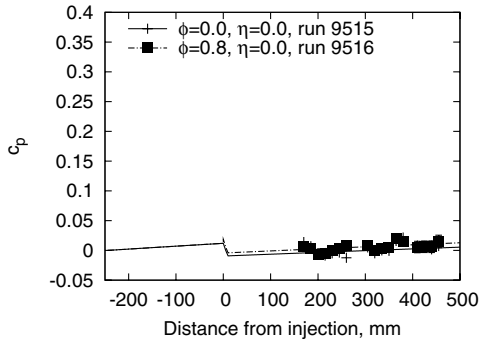

a) Long sharp configuration

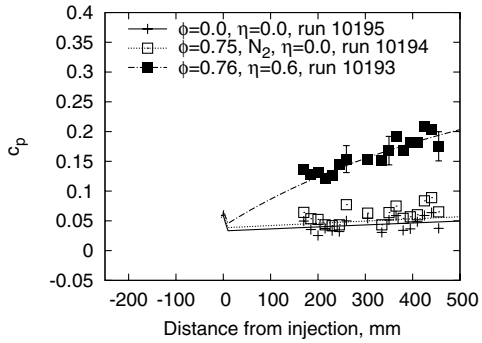

b) Short blunt configuration

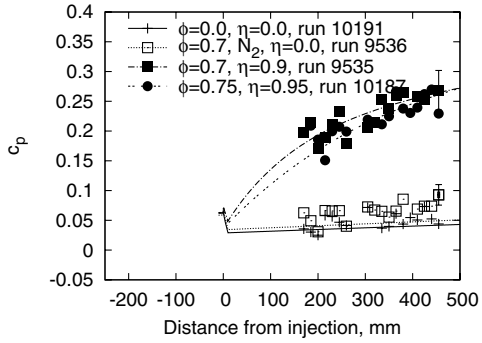

c) Long blunt configuration

Fig. 7 Cycle analysis and experimental pressure coefficient profiles for condition A. Symbols represent experimental data; lines represent one-dimensional prediction.

parameters of the shock tunnel p_{fill}, T_{fill}, u_s, and p_0 were measured and used to calculate the conditions of the gas just upstream of the nozzle throat. This is done with ESTCj, a python-coded successor of Equilibrium Shock Tube Conditions [43] using the Chemical Equilibrium with Applications [44] program to calculate the gas properties in thermal and chemical equilibrium. The resulting stagnated gas properties were passed to Nonequilibrium Nozzle Flow [45], a numerical code for the calculation of the flow expansion through a nozzle, assuming either equilibrium or nonequilibrium chemistry.

A detailed uncertainty analysis was carried out to estimate the uncertainties in the freestream conditions, following the procedure described in [46]. The numerical codes were run numerous times with slight perturbations in the measured quantities to assess the sensitivity of the derived quantities to these perturbations. This gives an indication of how the uncertainties in the measured quantities progress through the numerical processes and are amplified or attenuated. The product of this sensitivity and the uncertainty of a measured quantity yields the uncertainty of the derived quantity due to that of the measured quantity. The total uncertainty of each derived quantity is then found as the square root of the sum of squares of these individual uncertainties [46].

The pressure transducers in the duct were calibrated in situ, using an atmospherically driven shock-tube arrangement. The ends of the tubular combustion chamber were sealed and the tube almost evacuated. A sharp point was used to burst the thin membrane sealing one end, sending a shock wave into the tube. The pressure-time history was recorded by a piezoresistive pressure transducer that was calibrated against a dead weight tester. The voltage output of the duct sensors in relation to the measured pressure change yielded the respective sensitivities. A number of trials showed that these calibrations were repeatable to within $\pm 2.5\%$.

The pressure in the nozzle-supply region of the shock tunnel was measured using two piezoelectric pressure transducers that were shielded against temperature effects. These transducers were calibrated using a hydraulic rig that pressurizes the transducer and releases that pressure suddenly when a valve was opened. The calibration was made over a range of pressures and the standard deviation of the resulting calibration constant was less than 2% of the average value.

The start of the steady test flow is determined by the startup phenomena of the nozzle flow and the establishment of fully developed boundary layers on the model. This was taken as the time for the flow to travel three times the length of the model [47]. The combined startup time was 1.5 ms for the present tests. The end of the useful test time is dictated by contamination of the test gas by the driver gas. This has been investigated for flows in the T4 shock tunnel by several authors previously [48–51] and it was found that contamination occurs earlier for higher nozzle-supply enthalpies. Approximately 10% contamination occurs 2.5 ms after flow arrival for the highest enthalpy condition used in this investigation, condition D, and more than 4 ms after flow arrival for the lowest enthalpy condition, condition A. The static wall pressures were taken as the average value of the time-dependent pressure trace measured during the period of established steady flow.

Most of the pressure measurements in this paper are presented as pressure coefficients. Presenting results in this way helps to reduce the effects of shot-to-shot variations in conditions. The typical uncertainties in the coefficients are shown by sample error bars in Fig. 7. Shot-to-shot repeatability of the duct pressure coefficient for identical nominal freestream conditions was established to within $\pm 5\%$ for most transducers, although some showed variations as large as $\pm 10\%$. Pressure coefficients were computed using the derived freestream flow properties and measured static wall pressures.

B. Fuel-Injection Conditions

In the present configuration, fuel is injected near-tangentially from an annular slot underneath an established boundary layer. The slot has a converging–diverging area profile with an effective area ratio of 5.1, resulting in an injection Mach number of approximately 3.2. The downstream end of the nozzle is inclined at 17 deg to the mainstream flow, so that there is a component of the ejection velocity at the exit of the nozzle that is directed toward the center of the duct. However, the fuel-mass flow rates for all cases presented here were such that the fuel stream was strongly overexpanded. The overexpansion will result in the formation of a shock wave and its reflection from the wall just downstream of the nozzle, recompressing the fuel stream and initially deflecting it toward the wall before it is turned parallel to the mainstream. The key parameters specifying the nozzle exit conditions of the fuel are given in Table 2.

The mixing of the fuel with the air is clearly important for combustion, and there have been many studies into mixing of

Table 2 Nominal experimental fuel-injection conditions at the exit of the fuel-injection slot

Condition	ϕ	p_j	u_j	ρ_j
——	——	kPa	m/s	kg/m^3
A	0.8	9.3	2280	0.026
B	0.8	9.3	2280	0.026
B	1.5	16.0	2280	0.045
C	1.0	9.3	2280	0.026
D	1.0	9.3	2280	0.026

coflowing compressible streams. An upper bound for the mixing of two coflowing streams can be the growth rate of the shear layer that develops at the fluid interface [52]. However, the present experimental configuration results in a complex flowfield where the shear layer between the streams of fuel and air develops. Entropy and boundary layers upstream of the shear layer as well as shock and expansion waves that intersect this layer alter the mixing characteristics and are difficult to account for [53,54]. Additionally, the combustion chamber wall is in close proximity to the shear layer so that the shear layer can grow only until it reaches the wall. When fuel is injected into an airstream and combustion occurs, the release of heat in the shear layer slows the development of large-scale structures in the shear layer, lessening entrainment and hence, reducing mixing [55,56]. Similar effects are expected for boundary-layer combustion.

A simplified analysis, following the suggestions by Slessor et al. [57], was carried out to quantify some of the key mixing parameters. This indicated little difference in mixing between the conditions presented here. In light of the many flow characteristics that have a quantitatively undetermined effect on mixing, these differences are left unquantified.

V. Experimental Results

Experimental results are presented in Figs. 7–11 as pressure coefficient profiles along the streamwise axis of the combustor. Symbols represent measurements and lines represent estimates obtained with the cycle analysis program. Crosses are used for air test gas cases without fuel injection and open symbols for nitrogen test gas experiments with hydrogen injection. Filled symbols indicate that hydrogen was injected into air test gas. The values of η stated in the legend of the figures are the combustion efficiencies $\eta_{c,\mathrm{tot}}$ at the end of the combustor and were obtained as described in Sec. III.B. Results are shown in order of increasing enthalpy conditions, starting with the lowest enthalpy.

A. Condition A

The experimental data for condition A are summarized in Fig. 7. Figure 7a indicates no signs of a combustion-induced pressure rise for the long inlet configuration with a sharp leading edge. The corresponding experiments with a short inlet configuration were therefore not performed, because ignition would be even less likely with its thinner, laminar boundary layer. The level of the pressure coefficients calculated using the cycle analysis and a general trend of increasing pressure along the duct match well with the experimental results. The expansion at the step ($x = 0$) can be seen in the cycle analysis results. Pressure variations along the duct caused by the viscous interactions in the inlet and the step in the duct can be seen in the experiments but not in the results from the quasi-one-dimensional cycle analysis. The cycle analysis predicts c_p to be approximately 0.01 higher for the case with injection. This difference is associated with the flow displacement effect of the fuel injection. The difference is within the experimental uncertainty and is not clear in the experiments. However, such differences are evident in some of the other experiments.

Figures 7b and 7c show the effects of leading-edge bluntness on combustion. Ignition occurs upstream of the first pressure measurement location, but the positive slope of the pressure profile indicates ongoing combustion throughout the duct. The c_p level from the cycle analysis for the cases with blunted leading edges agrees well with the experimental values for the cases where no fuel was injected. The increased c_p levels with fuel injection into nitrogen are evident in the experiments and, in these cases, the increase is larger than is predicted by the cycle analysis. However, the differences are again within the experimental uncertainty. The wave structure that is apparent in the sharp leading-edge results can also be seen in the data for the blunt leading edges, but is more pronounced due to the stronger leading-edge shocks as seen in Fig. 3b and 4b. Results for two shots for ignition of hydrogen into air for similar fuel equivalence ratios are shown in Fig. 7c. This gives an indication of the repeatability of these experimental results (see Fig. 8b also). Because of the relatively low stagnation enthalpy and static temperature, combustion heat release is high. The combustion efficiency, as indicated by cycle analysis, is approximately 60% for the short blunt inlet case and much higher for the long blunt inlet configuration. However, these values may not be reliable because the resulting effective fuel equivalence ratio is not small [3,35,36].

These results indicate that fuel injected along the wall of this combustor will ignite when there is a relatively thick entropy layer upstream of the point of fuel injection and that almost complete combustion occurs for the long blunt inlet. Note that this result is for Mach 8 flight conditions with the dynamic pressure q_f as low as 17 kPa.

B. Condition B

Results from tests at condition B are shown in Fig. 8. Condition B has a higher stagnation enthalpy than condition A and, consequently, a higher static temperature in the duct. Results at this condition show that combustion occurs for the long sharp inlet configuration.

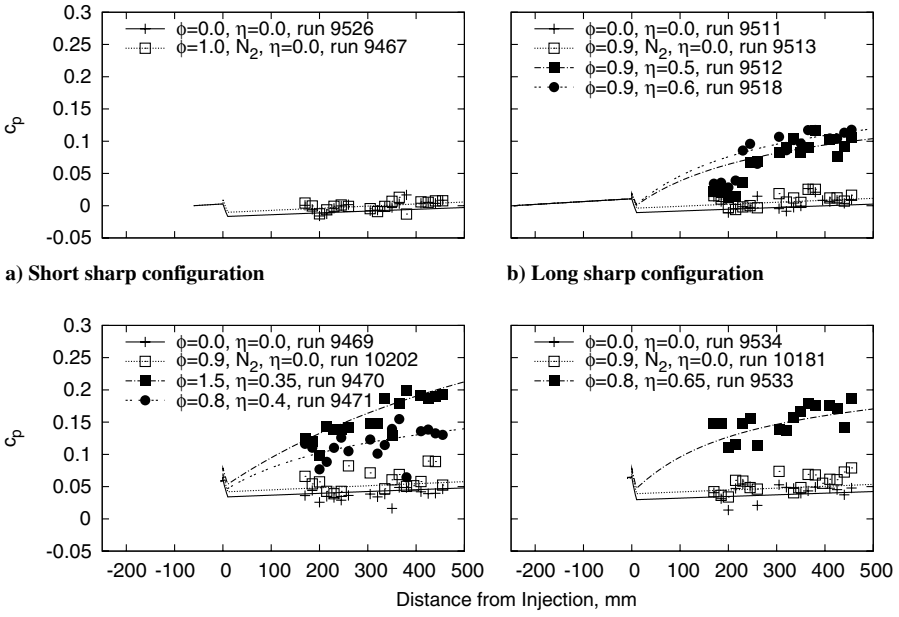

a) Short sharp configuration **b) Long sharp configuration**

c) Short blunt configuration **d) Long blunt configuration**

Fig. 8 Cycle analysis and experimental pressure coefficient profiles for condition B. Symbols represent experimental data; lines represent one-dimensional prediction.

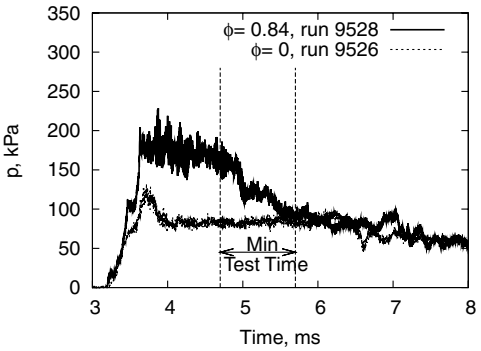

a) Unsustained combustion

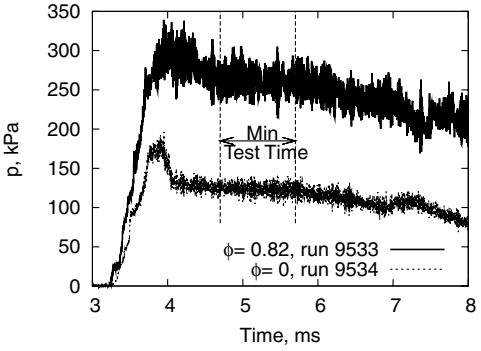

b) Sustained combustion

Fig. 9 Combustion induced pressure rises for a) the short sharp, and b) long blunt inlet configurations, approximately 380 mm downstream of injection. Test condition B.

Ignition occurs approximately 250 mm downstream of injection where the pressure coefficient profile rises suddenly away from the corresponding no-combustion profile. According to the cycle analysis, the measured pressure levels indicate that 50–60% of the injected fuel was consumed at the end of the duct. The sudden rise of pressure indicates that fuel and air were well mixed at the point of ignition and when ignition occurred, a large portion of the fuel burnt almost instantaneously. Combustion proceeded downstream of the ignition point, but was mixing limited.

The plot in Fig. 8a contains only pressure coefficient profiles for experiments with air test gas without injection and nitrogen test gas with injection. Corresponding experiments with injection into air test gas have been carried out and some combustion-induced pressure rise was evident in the time histories of pressure measurements. However, this pressure rise was not maintained for the full duration of the test time and when the pressure decreased, it dropped rapidly. Figure 9a shows one of these unsustained combustion cases, whereas Fig. 9b gives an example of a steady pressure trace from an experiment with a blunt leading edge at the same location and nominal condition. Corresponding no-injection traces are also shown.

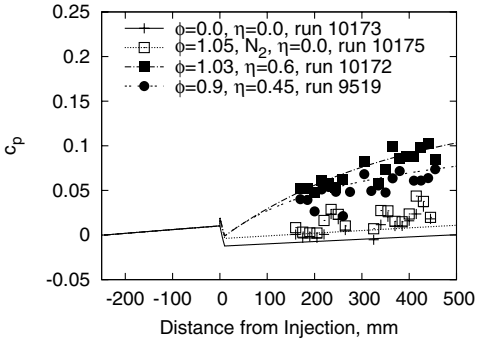

Fig. 10 Cycle analysis and experimental pressure coefficient profiles for condition C, long sharp configuration only. Symbols represent experimental data; lines represent one-dimensional prediction.

Figure 9a shows that, after a flow startup period of 1.5 ms, the pressure level for the fuel-injection case is steady for less than 1 ms and then drops to the no-injection value. This indicates that the fuel initially ignited, but the flame was extinguished quickly. One explanation for this could be the arrival of argon driver gas, contaminating the test flow. However, previous investigations indicate that a significant level of contamination will not occur for at least 3 ms after flow arrival for this condition [51]. Furthermore, if driver-gas contamination caused the flame extinction, this should occur earlier at higher nozzle-supply enthalpy conditions, resulting in an even shorter plateau of steady pressure. This was not observed for tests at enthalpies of 6.3 and 7.9 MJ/kg (see Figs. 10 and 11). The pressure level remains steady for more than 1.5 ms after the flow establishment time (2.5 ms after flow arrival corresponds to approximately 10% driver-gas contamination). It is therefore concluded that combustion is not sustained for the case of 5.3 MJ/kg with a short inlet with a sharp leading edge. Results from experiments with unsteady pressure time histories during the test time are not included in this paper and, therefore, Fig. 8a does not contain data from tests with fuel injection into air test gas. However, because Fig. 8b shows stable combustion in the downstream half of the combustor, it is concluded that a thicker, turbulent boundary layer at station 3 helps in maintaining stable combustion in the wall layer.

The no-combustion nitrogen test gas data in Figs. 8c and 8d show a similar pressure difference from the air test gas cases without injection to the corresponding data for condition A, and the predictions agree well with the experimental data. Combustion-induced pressure rise is evident for both the short and long inlet configurations with blunted leading edges. For the short blunt inlet, the pressure measurements indicate that combustion begins upstream of the first pressure measurement location and that the combustion pressure rise for the lower ($\phi = 0.8$) equivalence ratio experiment is significantly smaller than that of the experiment with $\phi = 1.5$. This means that more fuel was consumed at the higher equivalence ratio, suggesting that mixing is enhanced at the higher fuel-mass flow rate. Similar to the data shown in Fig. 7, the pressure rise (and combustion efficiency) is higher for the long blunt inlet configuration than for the short blunt configuration. The main difference between the long sharp and long blunt configuration is the location of ignition. This may be attributed, at least in part, to the higher temperatures and pressures in the duct for the blunt configuration. Note that, despite the larger ignition delay for the long sharp inlet compared with the long blunt inlet, the total amount of fuel burned is similar at the end of the duct.

C. Condition C

Experiments at condition C were not carried out for the entire range of model configurations. A full set of combustion data was only obtained for the long sharp configuration to complement the data shown in Fig. 8b, where ignition occurred approximately 250 mm downstream of injection. The pressure coefficient profiles for the long sharp configuration at condition C are shown in Fig. 10. The differences from the results shown in Fig. 8b are small for the combustion pressure profiles. The indicated combustion mass fraction is also comparable (between 45 and 60%), but the ignition location has moved upstream due to the increased static temperature in the core flow. Agreement between fuel-off measurements and cycle analysis predictions is not as good for this condition as it is for conditions A and B.

D. Condition D

The experimental results for condition D with the highest nozzle-supply enthalpy are shown in Fig. 11. The freestream static temperature for this condition reached almost 1800 K and the combustor entry temperature for the blunt leading-edge cases was estimated at approximately 2500 K. This resulted in ignition upstream of the first pressure measurement location and sustained combustion for all model configurations. The pressure rises due to combustion for the sharp inlet configurations (Fig. 11a and 11b) are relatively small, and little difference in combustion mass fraction is indicated between the short and long sharp configuration. The cycle

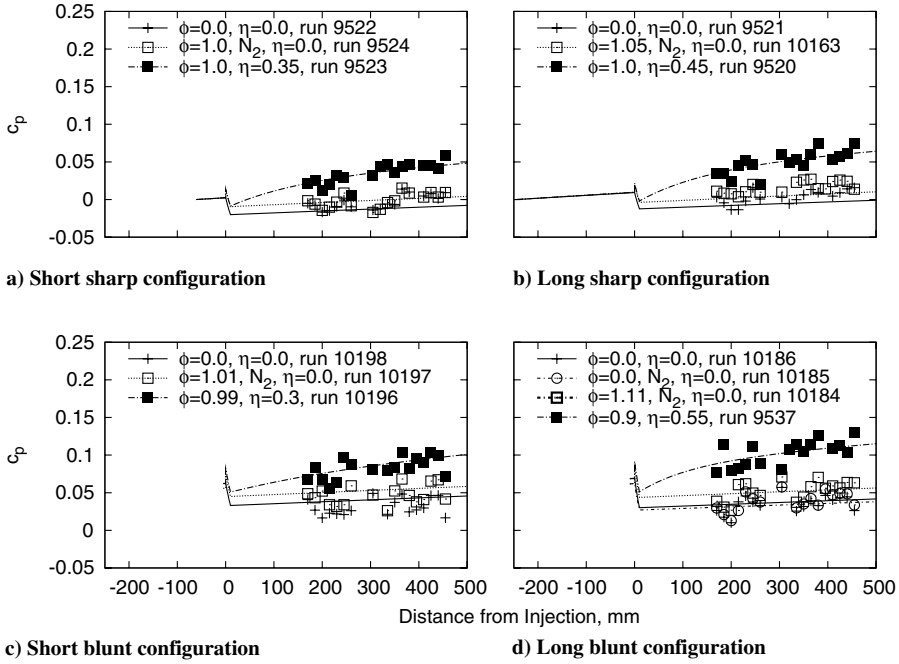

a) Short sharp configuration **b) Long sharp configuration**

c) Short blunt configuration **d) Long blunt configuration**

Fig. 11 Cycle analysis and experimental pressure coefficient profiles for condition D. Symbols represent experimental data; lines represent one-dimensional prediction.

analysis predicts the fuel-off pressure levels well for both, air and nitrogen test gas cases. Figure 11d shows a pressure profile for nitrogen test gas without injection as well as with injection. The effect of the mass addition is apparent when hydrogen is injected into a nitrogen test gas, but no appreciable difference is found between air and nitrogen test gas cases without injection.

The pressure rise and combustion efficiency indicated for the long blunt configuration is significantly higher than for the short blunt inlet case. It should be noted that the combustor exit temperature indicated by the cycle analysis code is approximately 2600 K for the short blunt inlet case and more than 2900 K for the long blunt case. It is possible that some of the combustion processes in the long blunt case are limited by this high temperature and some reactions are not completed. The combustion mass fractions indicated by the cycle analysis are lower than for the lower enthalpy conditions throughout. However, the results still show that more fuel is consumed at the end of the duct for increasing inlet length and bluntness.

Overall, the results at conditions A–D show that, when the fuel ignites, the proportion of fuel consumed at the end of the 500-mm-long combustor decreases as the equivalent flight Mach number increases.

E. Influence of Blunted Leading-Edge Shocks vs Entropy Layer

An attempt was made to reduce the influence on ignition and combustion of the relatively strong shock wave that originates from the blunted leading edge. To reduce the strength and increase the distance between impingement locations of this shock wave as it propagates down the duct, the inlet duct diameter was increased to 42.4 mm, resulting in nearly a doubling of the cross-sectional area of the combustor. The bluntness radius of the leading edge and the backward-facing step height were kept constant and the length of the inlet was the same as for the long inlet configuration of the small diameter duct. The fuel-mass flow rate per unit circumferential slot length was approximately the same for the small and large diameter ducts, meaning that the fuel-injection conditions were kept the same. The total equivalence ratio was smaller for the large diameter duct because the fuel-mass flow rate only increased linearly with the diameter, but the capture area increased with its square. This resulted in a smaller combustion-induced pressure rise for the same amount of heat release per unit area of internal combustor surface. To capture additional flow features, in particular the ignition location of the injected fuel, pressure measurements were taken closer to the injection location.

The axial pressure distributions for the large duct are shown in Figs. 12 and 13 for conditions A and B, respectively. Note the lower pressure rise for the large diameter duct when compared with the corresponding data for the small diameter duct (see Figs. 7c and 8d). The combustion efficiencies indicated by the one-dimensional analysis are also smaller and perhaps are, therefore, more reliable because the effective equivalence ratio is much smaller than unity.

Another method to compare the combustion achieved in the different diameter ducts is to model the pressure rise in the duct as

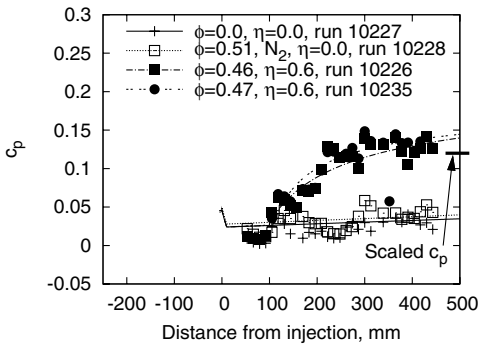

Fig. 12 Cycle analysis and experimental pressure coefficient profiles for condition A, large model diameter, blunt leading edge. Symbols represent experimental data; lines represent one-dimensional prediction.

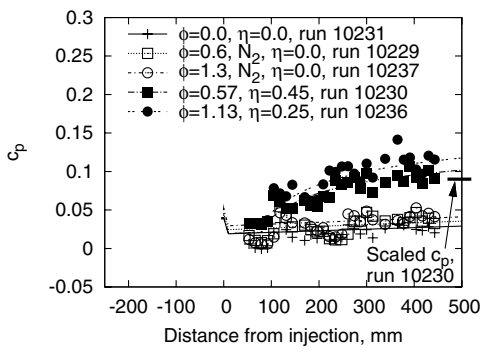

Fig. 13 Cycle analysis and experimental pressure coefficient profiles for condition B, large model diameter, blunt leading edge. Symbols represent experimental data; lines represent one-dimensional prediction.

being caused by increased displacement thickness of the wall layer due to combustion. The mainstream flow is then considered to be compressed by the restricted area. The pressure rise in the duct that is shown in Figs. 7c and 8d can be related to a change in Mach number if the compression is assumed to be isentropic (Eq. 44 of [58]). This change in Mach number can in turn be expressed in terms of an area change (Eq. 80 of [58]), which is caused by the combustion-induced increase of the boundary-layer displacement thickness. Because the wetted length upstream of station 3 and the fuel-injection conditions are the same for the large and small ducts, the conditions for boundary-layer combustion and the resulting displacement effect should be similar in the two ducts unless the effects of the shocks in the duct are strong. Because of the different duct diameters, the same displacement causes different pressure rises. The displacement thickness calculated from the pressure rise measured for the small duct was applied to the large diameter duct to estimate the pressure rise that results from this displacement. The resulting scaled pressure coefficients at the end of the duct are shown by horizontal bars in Figs. 12 and 13.

The pressure coefficients that are expected at the end of the large duct if the displacement effect due to combustion was the same for both duct diameters agree well with the experimental data. This suggests that the combustion heat release in the two ducts is similar and that the amount of fuel consumed in the small duct is similar to that for the large duct. It is concluded that the stronger and more closely spaced shocks impinging on the fuel layer for the small duct do not lead to significantly different combustion in the boundary layer. This also suggests that the combustion efficiencies inferred from the one-dimensional cycle analysis are indeed not reliable when the effective equivalence ratio is not significantly smaller than unity.

There is evidence that the ignition occurs for both conditions A and B when the bluntness-induced shock impinges on the fuel layer. Note the rapid increase in pressure for the fuel injection into air for both conditions at approximately 100 mm from injection.

VI. Conclusions

The current experimental data supports the initial proposition that entropy layers and thick, turbulent boundary layers at the entrance of a scramjet combustor can aid in ignition and combustion of boundary-layer injected hydrogen fuel. Blunted leading edges primarily promote ignition and, if combustion is started, affect the total amount of fuel consumed within the combustion chamber only marginally. A thick, turbulent boundary layer at the injection point can also aid in ignition and combustion (see Figs. 8 and 11). This is of importance, because the boundary layers on scramjet-powered flight vehicles will be growing for a long distance on the vehicle's forebody and the compression inlet. Flight vehicles will also have blunted leading edges to cope with high stagnation-point heat transfer rates and it is shown that these enhance ignition and enable combustion of wall-slot injected gaseous hydrogen at lower static temperatures than a sharp leading edge. These effects could aid in partly offsetting the detrimental effects that thick boundary layers and blunted leading edges have on vehicle drag and scramjet performance.

The experimental data generally show that less relative pressure rise is obtained when the same amount of fuel is burnt in a higher enthalpy environment. For conditions B–D, the indicated total combustion mass fraction did not change much for the same experimental configuration, but the point of ignition moved further upstream as the total enthalpy was increased (from approximately 230 mm to a point upstream of the first transducer location at 170 mm). The data for the lowest total enthalpy (condition A) stands out from the other data because no combustion was achieved for any sharp edge configurations. This clearly shows that blunted leading edges enable combustion to be achieved when there is no combustion for the sharp inlet cases. However, the shock waves generated by the blunted leading edges had a large influence, not only on the near wall temperature profile, but on the core flow in the combustor. This leads to higher pressures and densities in the duct, resulting in shorter ignition delay times [27].

A comparison of the results that were obtained for the large diameter duct with those of the small diameter duct with a blunted leading edge for conditions A and B suggests that the fuel layer was not disrupted significantly by the impinging shock waves that were generated by the bluntness, and that combustion did take place in the boundary layer. The one-dimensional cycle analysis fails to accurately predict the amount of fuel that is consumed at least for the low enthalpy conditions and where high-effective equivalence ratios are computed.

It was not possible to conclusively deduce the main source of ignition from the blunt leading-edge experimental data, but the results that were obtained with the large diameter duct indicate that ignition occurred near a point of shock impingement.

Acknowledgments

The support of the Australian Research Council under grant DP0665016 is gratefully acknowledged. The authors wish to thank Keith Hitchcock, Wilson Chan, Luke Doherty, Sarah Razzaqi, Andrew Ridings, James Turner, and Katsuyoshi Tanimizu for maintaining and operating the shock tunnel during the test campaigns.

References

[1] Stalker, R. J., and Morgan, R. G., "Parallel Hydrogen Injection into Constant-Area, High-Enthalpy, Supersonic Airflow," *AIAA Journal*, Vol. 20, No. 10, 1982, pp. 1468–1469. doi:10.2514/3.7987

[2] Rogers, R. C., Capriotti, D. P., and Guy, R. W., "Experimental Supersonic Combustion Research at NASA Langley," *20th AIAA Advanced Measurement and Ground Testing Technology Conference*, Albuquerque, NM, AIAA Paper 98-2506, June 1998.

[3] Billig, F. S., "Research on Supersonic Combustion," *Journal of Propulsion and Power*, Vol. 9, No. 4, 1993, pp. 499–514. doi:10.2514/3.23652

[4] Drummond, J. P., Diskin, G. S., and Cutler, A. D., "Fuel-Air Mixing and Combustion in Scramjets," *38th AIAA/ASME/SAE/ASEE Joint Propulsion Conference and Exhibit*, Indianapolis, IN, AIAA Paper 2002-3878, 2002.

[5] Seiner, J. M., Dash, S. M., and Kenzakowski, D. C., "Historical Survey on Enhanced Mixing in Scramjet Engines," *Journal of Propulsion and Power*, Vol. 17, No. 6, 2001, pp. 1273–1286. doi:10.2514/2.5876

[6] Bogdanoff, D. W., "Advanced Injection and Mixing Techniques for Scramjet Combustors," *Journal of Propulsion and Power*, Vol. 10, No. 2, 1994, pp. 183–190. doi:10.2514/3.23728

[7] Yates, C. L., "Two-Dimensional Supersonic Mixing of Hydrogen and Air Near a Wall," NASA Contractor Rept. NASA-CR-1793, Johns Hopkins Univ., Silver Springs, MD, March 1971.

[8] Rowan, S. A., and Paull, A., "Performance of a Scramjet Combustor with Combined Normal and Tangential Fuel Injection," *Journal of Propulsion and Power*, Vol. 22, No. 6, 2006, pp. 1334–1338. doi:10.2514/1.18744

[9] Northam, G. B., Greenberg, I., Byington, C. S., and Capriotti, D. P., "Evaluation of Parallel Injector Configurations for Mach 2 Combustion," *Journal of Propulsion and Power*, Vol. 8, No. 2, March–April 1992, pp. 491–499. doi:10.2514/3.23503

[10] Eckert, E. R. G., "Gas-to-Gas Film Cooling," *Journal of Engineering Physics and Thermophysics*, Vol. 19, No. 3, 1970, pp. 1091–1101. doi:10.1007/BF00826233

[11] Cary, A.M. J., and Hefner, J. N., "Film-Cooling Effectiveness and Skin Friction in Hypersonic Turbulent Flow," *AIAA Journal*, Vol. 10, No. 9, Sept. 1972, pp. 1188–1192. doi:10.2514/3.50348

[12] Odam, J., and Paull, A., "Radical Farming in Scramjets," *New Results in Numerical and Experimental Fluid Mechanics VI*, edited by C. Tropea, Notes on Numerical Fluid Mechanics and Multidisciplinary Design, Springer–Verlag, New York, 2007, pp. 276–283.

[13] Anderson, J. D., Jr., *Hypersonic and High Temperature Gas Dynamics*, McGraw–Hill Series in Aeronautical and Aerospace Engineering, McGraw–Hill, New York, 1989.

[14] Suraweera, M. V., Mee, D. J., and Stalker, R. J., "Skin-Friction Reduction in Hypersonic Turbulent Flow by Boundary-Layer Combustion," *43rd AIAA Aerospace Sciences Meeting and Exhibit*, Reno, NV, AIAA Paper 2005-613, 2005.

[15] Stephensen, D. J., "Controlling Skin Friction by Boundary-Layer Combustion," Undergrad. Eng. Thesis, Dept. of Mechanical Engineering, Univ. of Queensland, Brisbane, Australia, Nov. 2002.
[16] Schetz, J. A., and Favin, S., "An Analysis of the Ignition of Slot-Injected Gaseous Hydrogen in a Supersonic Air Stream," *Combustion and Flame*, Vol. 11, No. 5, Oct. 1967, pp. 397–407. doi:10.1016/0010-2180(67)90060-0
[17] Kovachevich, A., Paull, A., and McIntyre, T., "Investigation of an Intake Injected Hot-Wall Scramjet," *42nd AIAA Aerospace Meeting and Exhibit*, Reno, NV, AIAA Paper 2004-1037, 2004.
[18] van Driest, E. R., "Turbulent Boundary Layer in Compressible Fluids," *Journal of the Aeronautical Sciences*, Vol. 18, No. 3, March 1951, pp. 145–160.
[19] Stalker, R. J., "Recent Developments with Free Piston Drivers," *Proceedings of the 17th International Symposium on Shock Waves and Tubes*, Current Topics in Shock Waves, Vol. 208, American Inst. of Physics, Bethlehem, PA, 1990, pp. 96–107.
[20] Jacobs, P. A., and Stalker, R. J., "Mach 4 and Mach 8 Axisymmetric Nozzles for a Shock Tunnel," NASA Contractor Rept. NASA-CR 187533;Institute for Computer Applications in Science and Engineering, Rept. 91-24, NASA Langley Research Center, Feb. 1991.
[21] Kirchhartz, R. M., Mee, D. J., and Stalker, R. J., "Skin Friction Drag with Boundary Layer Combustion in a Circular Combustor," *15th AIAA International Space Planes and Hypersonic Systems and Technologies Conference*, Dayton, OH, AIAA Paper 2008-2589, April 2008.
[22] Jacobs, P. A., "MB_CNS: A Computer Program for the Simulation of Transient Compressible Flows," Dept. of Mechanical Engineering, Rept. 10/96, Univ. of Queensland, Brisbane, Australia, Dec. 1996.
[23] He, Y., and Morgan, R. G., "Transition of Compressible High Enthalpy Boundary Layer Flow over a Flat Plate," *Aeronautical Journal*, Vol. 98, No. 972, 1994, pp. 25–34.
[24] Mee, D. J., "Boundary-Layer Transition Measurements in Hypervelocity Flows in a Shock Tunnel," *AIAA Journal*, Vol. 40, No. 8, 2002, pp. 1542–1548. doi:10.2514/2.1851
[25] Baldwin, B. S., and Lomax, H., "Thin Layer Approximation and Algebraic Model for Separated Turbulent Flows," *AIAA 16th Aerospace Sciences Meeting*, Huntsville, AL, AIAA Paper 78-257, 1978.
[26] Korkegi, R. H., "A Lower Bound for Three-Dimensional Turbulent Separation in Supersonic Flow," *AIAA Journal*, Vol. 23, No. 3, March 1985, pp. 475–476. doi:10.2514/3.8938
[27] Rogers, R. C., and Schexnayder, C. J., "Chemical Kinetic Analysis of Hydrogen-Air Ignition and Reaction Times," NASA Technical Paper NASA-TP-1856, NASA Langley Research Center, Hampton, VA, July 1981.
[28] Heiser,W. H., and Pratt, D. T., *Hypersonic Airbreathing Propulsion*, AIAA Education Series, AIAA, Washington, D.C., 1994.
[29] Curran, E. T., and Craig, R. R., "The Use of Stream Thrust Concepts for the Approximate Evaluation of Hypersonic Ramjet Engine Performance," Tech. Rept. AFAPL-TR-73-38, Air Force Aero Propulsion Lab, Wright-Patterson AFB, OH, July 1973.
[30] d'Incà, R., and Bouchez, M., "Use of the SCHOLAR Supersonic Combustion Data: 1-D Analysis of the SCHOLAR Experiment," *Technologies for Propelled Hypersonic Flight*, NATO TR-AVT-007, Vol. 2, NATO Research and Technology Organization, Neuilly, France, 2006, Chap. 8.
[31] Murthy, S. N. B., "Basic Performance Assessment of Scram Combustors," *Scramjet Propulsion*, edited by E. T. Curran, and S. N. B. Murthy, Vol. 189, of Progress in Aeronautics and Astronautics, AIAA, Washington, D.C., 2000, Chap. 10, pp. 597–695.
[32] Anderson, G. Y., and Gooderum, P. B., "Exploratory Tests of Two Strut Fuel Injectors for Supersonic Combustion," NASA Technical Note NASA-TN-D-7581, NASA Langley Research Center, Feb. 1974.
[33] Riggins, D. W., "Evaluation of Performance Loss Methods for High-Speed Engines and Engine Components," *Journal of Propulsion and Power*, Vol. 13, No. 2, March 1997, pp. 296–304. doi:10.2514/2.5162
[34] Rogers, R. C., and Eggers, J. M., "Supersonic Combustion of Hydrogen Injected Perpendicular to a Ducted Vitiated Airstream," *AIAA Journal*, Vol. 12, No. 12, Dec. 1974, pp. 1621–1622. doi:10.2514/3.49569
[35] Billig, F. S., "Combustion Processes in Supersonic Flow," *Journal of Propulsion and Power*, Vol. 4, No. 3, May–June 1988, pp. 209–216. doi:10.2514/3.23050
[36] Heiser,W. H., and Pratt, D. T., "Aerothermodynamics of the Dual-Mode Combustion System," *Scramjet Propulsion*, edited by E. T. Curran, and S. N. B. Murthy, Vol. 189, of Progress in Aeronautics and Astronautics, AIAA, Washington, D.C., 2000, Chap. 9, pp. 569–595.
[37] Smart, M. K., "Scramjets," *Aeronautical Journal*, Vol. 111, No. 1124, Oct. 2007, pp. 605–619.
[38] Hornung, H. G., "28th Lanchester Memorial Lecture—Experimental Real-Gas Hypersonics," *Aeronautical Journal*, Vol. 92, No. 920, Dec. 1988, pp. 379–389.
[39] Smart, M. K., and Tetlow, M. R., "Orbital Delivery of Small Payloads Using Hypersonic Airbreathing Propulsion," *Journal of Spacecraft and Rockets*, Vol. 46, No. 1, Jan.–Feb. 2009, pp. 117–125. doi:10.2514/1.38784
[40] Stalker, R. J., Paull, A., Mee, D. J., Morgan, R. G., and Jacobs, P. A., "Scramjets and Shock Tunnels: The Queensland Experience," *Progress in Aerospace Sciences*, Vol. 41, No. 6, Aug. 2005, pp. 471–513. doi:10.1016/j.paerosci.2005.08.002
[41] Van Wie, D. M., "Scramjet Inlets," *Scramjet Propulsion*, edited by E. T. Curran, and S. N. B. Murthy, Vol. 189, of Progress in Astronautics and Aeronautics, AIAA, Washington, D.C., 2000, Chap. 7, pp. 447–511.
[42] IHS ESDU International plc, "Equations for Calculation of International Standard Atmosphere and Associated Off-Standard Atmospheres," ESDU Performance Series ESDU 77022, No. 3, 2008.
[43] McIntosh, M. K., "Computer Program for the Numerical Calculation of Frozen and Equilibrium Conditions in Shock Tunnels," Dept. of Physics Rept., Australian National Univ., Canberra, Australia, 1968.
[44] McBride, B. J., Zehe, M. J., and Gordon, S., "NASA Glenn Coefficients for Calculating Thermodynamic Properties of Individual Species," NASA Technical Paper NASA-TP-2002-211556, NASA John H. Glenn Research Center, Sept. 2002.
[45] Lordi, J. A., Mates, R. E., and Moselle, J. R., "Computer Program for the Numerical Simulation of Non-Equilibrium Expansions of Reaction Gas Mixtures," NASA Contractor Rept. NASA-CR-472, Cornell Aeronautical Lab., Buffalo, NY, 1966.
[46] Mee, D. J., "Uncertainty Analysis of Conditions in the Test Section of the T4 Shock Tunnel," Dept. of Mechanical Engineering, Research Rept. 4/39, Univ. of Queensland, 1993.
[47] Jacobs, P. A., Rogers, R. C., Weidner, E. H., and Bittner, R. D., "Flow Establishment in a Generic Scramjet Combustor," *Journal of Propulsion and Power*, Vol. 8, No. 4, July–Aug. 1992, pp. 890–899. doi:10.2514/3.23566
[48] Paull, A., and King, M. D., "A Driver Gas Detection Device for Shock Tunnels," *Shock Waves* , Vol. 4, No. 5, March 1995, pp. 289–291. doi:10.1007/BF01416041
[49] Paull, A., "A Simple Shock Tunnel Driver Gas Detector," *Shock Waves*, Vol. 6, No. 5, 1996, pp. 309–312. doi:10.1007/BF02535744
[50] Skinner, K. A., "Mass Spectrometry in Shock Tunnel Experiments of Hypersonic Combustion," Ph.D. Thesis, Univ. of Queensland, Dept. of Mechanical Engineering, Brisbane, Australia, 1994.
[51] Boyce, R. R., Takahashi, M., and Stalker, R. J., "Mass Spectrometric Measurements of Driver Gas Arrival in the T4 Free-Piston Shock-Tunnel," *Shock Waves*, Vol. 14, No. 5–6, Dec. 2005, pp. 371–378. doi:10.1007/s00193-005-0276-3
[52] Dimotakis, P. E., "Turbulent Free Shear LayerMixing and Combustion," *High-SpeedFlight Propulsion Systems*, Vol. 137, of Progress in Astronautics and Aeronautics, AIAA, Washington, D.C., 1991, Chap. 5, pp. 265–340.
[53] Gutmark, E. J., Schadow, K. C., and Yu, K. H., "Mixing Enhancement in Supersonic Free Shear Flows," *Annual Review of Fluid Mechanics*, Vol. 27, Jan. 1995, pp. 375–417. doi:10.1146/annurev.fl.27.010195.002111
[54] Parent, B., and Sislian, J. P., "Hypersonic Mixing Enhancement by Compression at a High Convective Mach Number," *AIAA Journal*, Vol. 42, No. 4, April 2004, pp. 787–795. doi:10.2514/1.9559
[55] McMurtry, P. A., Jou, W.-H., Riley, J. J., and Metcalfe, R. W., "Direct Numerical Simulations of a Reacting Mixing Layer with Chemical Heat Release," *AIAA Journal*, Vol. 24, No. 6, June 1986, pp. 962–970. doi:10.2514/3.9371
[56] McMurtry, P. A., Riley, J. J., and Metcalfe, R. W., "Effects of Heat Release on the Large-Scale Structure in Turbulent Mixing Layers," *Journal of Fluid Mechanics*, Vol. 199, Feb. 1989, pp. 297–332. doi:10.1017/S002211208900039X
[57] Slessor, M. D., Zhuang, M., and Dimotakis, P. E., "Turbulent Shear-LayerMixing: Growth-Rate Compressibility Scaling," *Journal of Fluid Mechanics*, Vol. 414, No. , July 2000, pp. 35–45. doi:10.1017/S0022112099006977
[58] Ames Research Staff, "Equations, Tables and Charts for Compressible Flow," NASA, Rept. 1135, 1953.

R. Bowersox
Associate Editor